

A Lagrangian view of moisture transport related to the heavy rainfall of July 2020 in Japan: Importance of the moistening over the subtropical regions

Ning Zhao¹, Atsuyoshi Manda², Xiaojun Guo³, Kazuyoshi Kikuchi⁴, Tomoe Nasuno⁵, Masuo Nakano¹, Yuanxin Zhang⁶, and Bin Wang⁷

¹Japan Agency for Marine-Earth Science and Technology

²Mie University

³University of Hawaii

⁴International Pacific Research Center, University of Hawaii

⁵Frontier Research Center for Global Change

⁶Tokyo University of Marine Science and Technology

⁷Hohai University

November 26, 2022

Abstract

The transport and accumulation of moisture played an essential role in the extremely heavy rainfall of July 2020 in Japan. To better understand this event in terms of moisture sources and transport routes, backward particle trajectory analysis was conducted. We found two major moisture sources: transport from the tropics and uptake from the subtropics. A narrow moisture channel was found along the edge of the western Pacific Subtropical High (WPSH), transporting the moisture to the Baiu front. However, most moisture from the tropics was lost due to precipitation, and their contributions were reduced to about 15%. In contrast, the subtropical regions contributed over 80% moisture via evaporation and lower tropospheric convection. Among those regions, the western Pacific contributed the most (33 %). This study highlights the role of WPSH in moisture transport, and also demonstrated the importance of the moisture uptake during the transport.

1 **A Lagrangian view of moisture transport related to the heavy rainfall of July 2020 in**
2 **Japan: Importance of the moistening over the subtropical regions**

3
4 **N. Zhao¹, A. Manda², X. Guo³, K. Kikuchi³, T. Nasuno¹, M. Nakano¹, Y. Zhang⁴, B. Wang⁵**

5 ¹ Research Institute for Global Change, Japan Agency for Marine-Earth Science and Technology,
6 Yokosuka, 2370061, Japan.

7 ² Earth and Environmental Sciences Division, Graduate School of Bioresources, Mie University,
8 Mie, 5148507, Japan.

9 ³ International Pacific Research Center, School of Ocean and Earth Science and Technology,
10 University of Hawaii, Honolulu, 96822, USA.

11 ⁴ Graduate School of Marine Science and Technology, Tokyo University of Marine Science and
12 Technology, Tokyo, 1088477, Japan.

13 ⁵ College of Oceanography, Hohai University, Nanjing, 210098, China.

14
15 Corresponding author: Ning Zhao (zhaoning@jamstec.go.jp)

16
17 **Key Points:**

- 18 • Moisture came from both the tropical regions and subtropical regions
- 19 • The western Pacific Subtropical High is major forcing of moisture transport and also
20 helped the moistening of low-level flows
- 21 • Subtropical regions (especially the western Pacific) contributed the most to the moisture
22 accumulation
23

24 **Abstract**

25 The transport and accumulation of moisture played an essential role in the extremely heavy
26 rainfall of July 2020 in Japan. To better understand this event in terms of moisture sources and
27 transport routes, backward particle trajectory analysis was conducted. We found two major
28 moisture sources: transport from the tropics and uptake from the subtropics. A narrow moisture
29 channel was found along the edge of the western Pacific Subtropical High (WPSH), transporting
30 the moisture to the Baiu front. However, most moisture from the tropics was lost due to
31 precipitation, and their contributions were reduced to about 15%. In contrast, the subtropical
32 regions contributed over 80% moisture via evaporation and lower tropospheric convection.
33 Among those regions, the western Pacific contributed the most (33 %). This study highlights the
34 role of WPSH in moisture transport, and also demonstrated the importance of the moisture
35 uptake during the transport.

36 **Plain Language Summary**

37 Heavy rainfalls hit Japan in July 2020, and the related atmospheric river was found to be
38 accumulated by the moisture from tropics and subtropics. The moisture was transported by a
39 narrow moisture channel along the edge of western Pacific Subtropical High. But, due to the
40 precipitation during the transport, the moisture from tropics decreased. On the other hand, when
41 the air flows passed over the subtropical regions, they were moistened by evaporation and lower
42 troposphere convection. Thus, our results suggest that the moisture from subtropical regions
43 contributed the most in the moisture accumulation during the heavy rain event.

44 **1 Introduction**

45 Extremely heavy rain fell over Japan in July 2020 (hereafter, 20HR). The rainfall
46 continued during this whole period and included several severe rainfall events. As reported by
47 the Japan Meteorological Agency (JMA), during this event, the 48 hr precipitation exceeded
48 1300 mm in many regions of western Japan (e.g., Kyushu, Gifu, Kochi, and Nagano).
49 Specifically, some records indicate that the total precipitation was equal to nearly half of the
50 historical annual mean (e.g., Fukuoka, Kagoshima) (JMA, 2020). It was reported that 82
51 fatalities occurred, and 18,380 buildings were destroyed or damaged during the heavy rains
52 (EOCJ, 2020).

53 Kamae (2020), based on a series of early analyses using the Japanese 55 year Reanalysis,
54 showed that a narrow plume of water vapor transport (i.e., the atmospheric river, AR; also see
55 Figure 1a) played a key role in the 20HR. According to the results in Kamae (2020) and JMA
56 (2020), this AR started from the South China Sea (SCS) and passed through the southeast China
57 mainland, before turning west along the Baiu front. It was also reinforced by the low level flows
58 from the south, similar to the previous heavy rains in Japan (e.g., Shimpo et al., 2019;).
59 Meanwhile, it is likely that the westward extension of the western Pacific Subtropical High
60 (WPSH) also enhanced the northward moisture transport from the SCS to Japan (e.g., Naoi et al.,
61 2020).

62 To date, the relationship between moisture transport and heavy rainfall during the Baiu
63 season has been extensively studied (e.g., Zhou & Yu, 2005; Tsuji & Takayabu, 2019). Most
64 studies have focused on the highly accumulated moisture itself (hence, the AR; e.g., Sampe &
65 Xie, 2010; Guan & Waliser, 2019; Shimpo et al., 2019), but few of them paid attention to why
66 such a massive amount of moisture accumulated and how was moisture transported (e.g., Bao et

67 al., 2006; Sodemann & Stohl, 2013). As to the winter time ARs associated with extratropical
 68 cyclones, Bao et al. (2006) showed that the local moisture convergence associated with the warm
 69 conveyor belt (WCB) and cold fronts is the fundamental force of the cyclone related ARs, and
 70 they also uncovered the vigorous moisture gain/loss processes during the transport. Sodemann
 71 and Stohl (2013) further emphasized the essential role of the WCB airstream in the formation
 72 and maintenance of AR. However, even the strong convergence also occurred and helped the
 73 moisture accumulation near the Baiu front during the heavy rain (JMA, 2020), it remains unclear
 74 how moisture was transported to Japan, especially considering that the 20HR was preceded by
 75 the heavy rainfalls (hence, the great moisture loss) over southeastern China where the AR likely
 76 passed (e.g., Zhong, 2020, JMA 2020).

77 This study addresses two scientific topics: (1) the moisture sources of AR and transport
 78 routes and (2) moisture gain/loss processes along the routes. Since an Eulerian point of view has
 79 limitations to clarify the sources of moisture and the processes affecting moisture accumulation
 80 of AR (see Gimeno et al., 2012 and references therein), we performed a Lagrangian experiment
 81 based on backward trajectories, which have proven to be computationally efficient and useful in
 82 similar studies (e.g., Sodemann et al., 2008; Langhamer et al., 2018). We carried out a numerical
 83 hindcast to obtain high-resolution atmospheric fields for backward tracing and to evaluate the
 84 physical details. Due to the complexity of the multiple events during the 20HR, this study was
 85 based on one major precipitation event (3–4 July in Kyushu; hereafter 20HR1) that caused a
 86 flooding disaster (NHK World News, 2020).

87 This paper is organized as follows. Section 2 describes the numerical hindcast, backward
 88 trajectory experiment, and diagnostic variables for analyses. Subsections in Sec. 3 document the
 89 results, including the moisture sources, routes, and gain/loss processes during transport. The
 90 major findings are summarized in Sec. 4.

91 **2 Materials and Methods**

92 **2.1 Numerical hindcast**

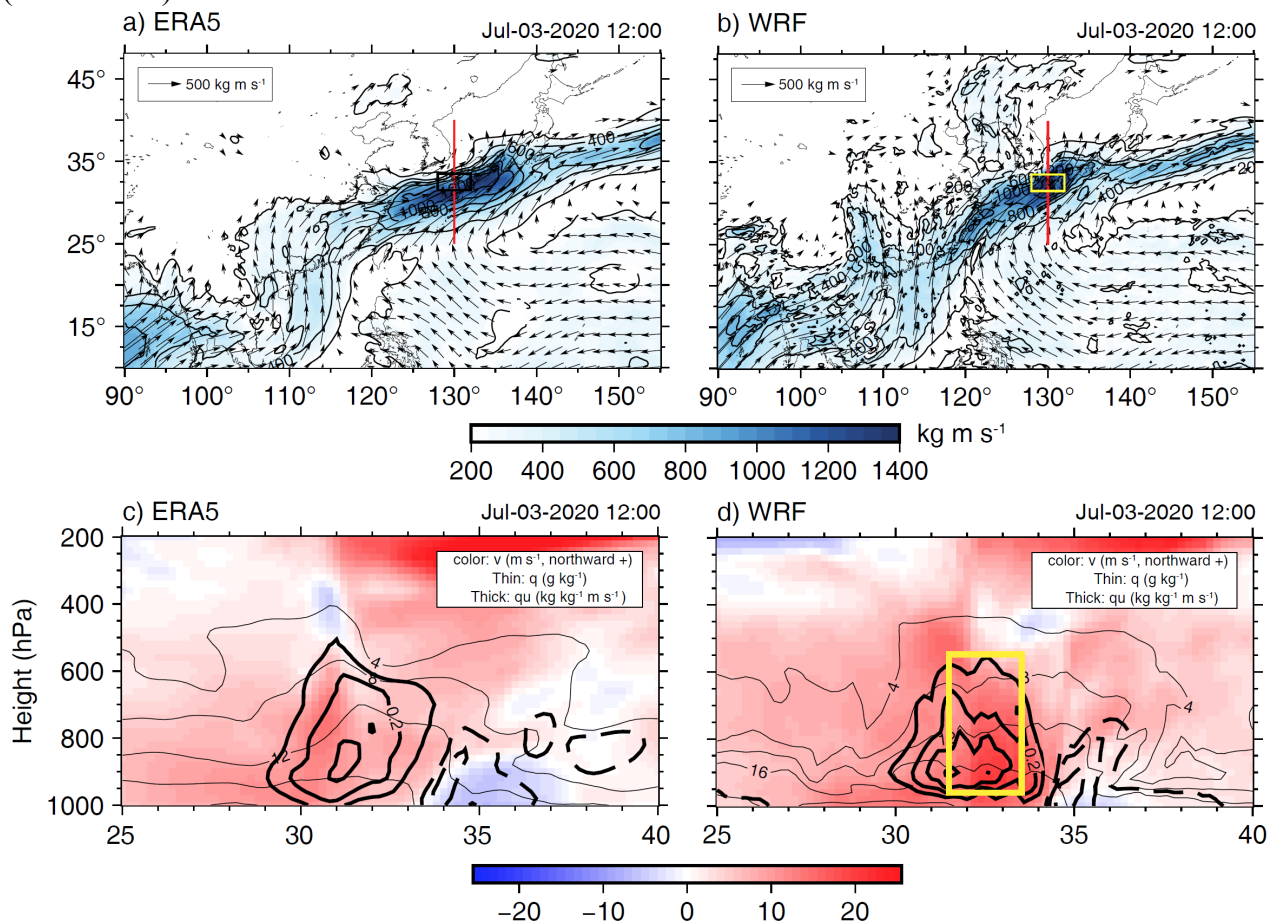
93 To obtain high spatial and temporal resolution atmospheric fields for the backward
 94 trajectories, we performed a numerical hindcast based on the Weather Research and Forecasting
 95 model (WRF V4.1.5). Our model covered the East Asian region (Figure 1), with 9-km mesh
 96 grids and 60 sigma layers from the surface to the top (50 hPa). The hindcast started from 27 June
 97 to 5 July. The boundary and initial conditions were interpolated from the 0.25-degree 6 hourly
 98 NCEP GDAS/FNL dataset (NCEP, 2015) and the sea surface temperature (SST) from the daily
 99 GHRSSST MultiProduct Ensemble (Martin et al., 2012). The output was saved every 30 minutes,
 100 and the first day was for spin-up and not used. We use the WSM6 microphysics scheme (Hong &
 101 Lim, 2006), the Yonsei University PBL scheme (Hong et al., 2006), the Revised MM5 surface
 102 layer scheme (Jimenez et al., 2012), the United Noah Land Surface Model (Tewari et al., 2004),
 103 the RRTMG Shortwave and Longwave Schemes (Iacono et al., 2008), and the Grell–Freitas
 104 Ensemble cumulus scheme (Grell & Freitas, 2014).

105 To clearly represent the moisture transport and to validate the WRF output, we calculated
 106 the IVT that have been commonly used in previous studies (e.g., Lavers et al., 2012):

$$107 \quad IVT = \sqrt{\left(\frac{1}{g} \int_{1000 \text{ hPa}}^{200 \text{ hPa}} qu \, dp\right)^2 + \left(\frac{1}{g} \int_{1000 \text{ hPa}}^{200 \text{ hPa}} qv \, dp\right)^2}, \quad (1)$$

108 where g is the gravitational acceleration, q is the specific humidity, p is the pressure, u and v are
 109 the zonal and the meridional wind, respectively.

110 We used the ERA5 reanalysis dataset (C3S, 2017) for model validation and comparison.
 111 As shown in Figure 1, our hindcast well reproduced the extremely high IVT, with strong water
 112 vapor fluxes from the surface to approximately 500 hPa. Our model showed good agreement
 113 with two satellite-based precipitation datasets in the localized heavy rain over the Kyushu (see
 114 Figure S1). Note that, although our model showed approximately 1 degree northward shift of the
 115 front and a lesser northward tilt with height (Figure 1), extra analyses demonstrated that the
 116 conclusions of this study were not sensitive to these mismatches and parameterizations we chose
 117 (see Text S1).



118
 119 **Figure 1.** The vertically integrated water vapor transport (IVT, panels a and b) and vertical cross
 120 sections (panels c and d) along the 130 E on 3 July, 12 UTC based on ERA5 and WRF (FNL
 121 based). Yellow boxes show the region for particle releasing, and red lines in upper panels show
 122 the location of cross section.

123 2.2 Backward trajectories

124 To identify the moisture source and transport route, we applied a backward trajectory
 125 analysis of the passive particles based on the FLEXPART-WRF model (Version 3.3.2; Brioude
 126 et al., 2013), which has been widely used in studies on moisture transport (e.g., Langhamer et al.,

127 2018). We used the snapshot wind obtained from WRF and the Hanna scheme as recommended
 128 by Brioude et al. (2013) for the turbulence parameterization, with the convection scheme on.

129 Particles were released from 3rd July, 00 UTC to 4th July, 12 UTC during the 20HR1 with
 130 a 12 hr interval over Kyushu from the 950 hPa to the 550 hPa height level, where the strong
 131 water vapor fluxes located (129–132 E and 31.5–33.5 N; boxes in Figure 1). Each particle
 132 represented an air parcel with specific mass, and 10,000 particles (with total mass of 20 kg) were
 133 released in this study. All particles were backward traced to 28th June, and their locations and
 134 properties would not change again when they reached a boundary. Because this study focused on
 135 the moisture transport, we excluded particles originated north of 30 N, which are generally dry
 136 and cold particles. As a result, 8868 particles remained for further analyses.

137 2.3 Diagnostic variables

138 Changes in the moisture content of a specific particle i (ΔQ_i) predominantly reflect the
 139 effects of precipitation (p) and evaporation (e) processes (e.g., Stohl and James, 2004):

$$140 \quad \Delta Q_{i,t} \approx Q_{i,t} - Q_{i,t-\Delta t} = \frac{m_{i,t}q_{i,t} - m_{i,t-\Delta t}q_{i,t-\Delta t}}{\Delta t} = e - p, \quad (2)$$

141 where $m_{i,t}$ is the mass of particle, $q_{i,t}$ is the specific humidity, t is time, Δt is the time interval
 142 (i.e., 30 mins), and $t = 0$ is the release time. For simplicity, the moisture uptake is regarded as
 143 $\Delta Q_{i,t} > 0$, and the precipitation is defined when $\Delta Q_{i,t} < 0$. Specifically, if moisture uptake
 144 occurred within the planetary boundary layer (PBL; obtained from WRF), a bulk evaporative
 145 moisture source (E) is identified, and we also adopted a factor of 1.5 to account for the potential
 146 underestimation and small scale variations of PBL.

147 To better evaluate the contribution of different moisture sources, we applied the ‘source
 148 attribution’ method as introduced by Sodemann et al. (2008). The general conception of this
 149 method is: a) once moisture uptake is detected, its weighted contribution would be determined
 150 ($f_{i,t} = \Delta Q_{i,t}/Q_{i,t}$), and all previous contributions will be diluted; and b) if precipitation is
 151 detected, all previously gained moisture will be reduced according to the weighted contributions.
 152 In simple terms, moisture uptake at previous times would be ‘filtered’ by precipitation occurred
 153 later (i.e., ‘rain-off’). Readers may refer to Text S2 for an example iteration for this method and
 154 Sodemann et al. (2008) for detailed descriptions.

155 The ‘rain-off’ filtered moisture uptake ($\Delta Q_{i,t,rain-off}$) for all particles in a specific
 156 atmospheric column yielded the final contribution for the accumulated moisture over the Kyushu
 157 region:

$$158 \quad \Delta Q_{tot} \approx \frac{\sum_1^N (\Delta Q_{i,t,rain-off})}{A}, \quad (3)$$

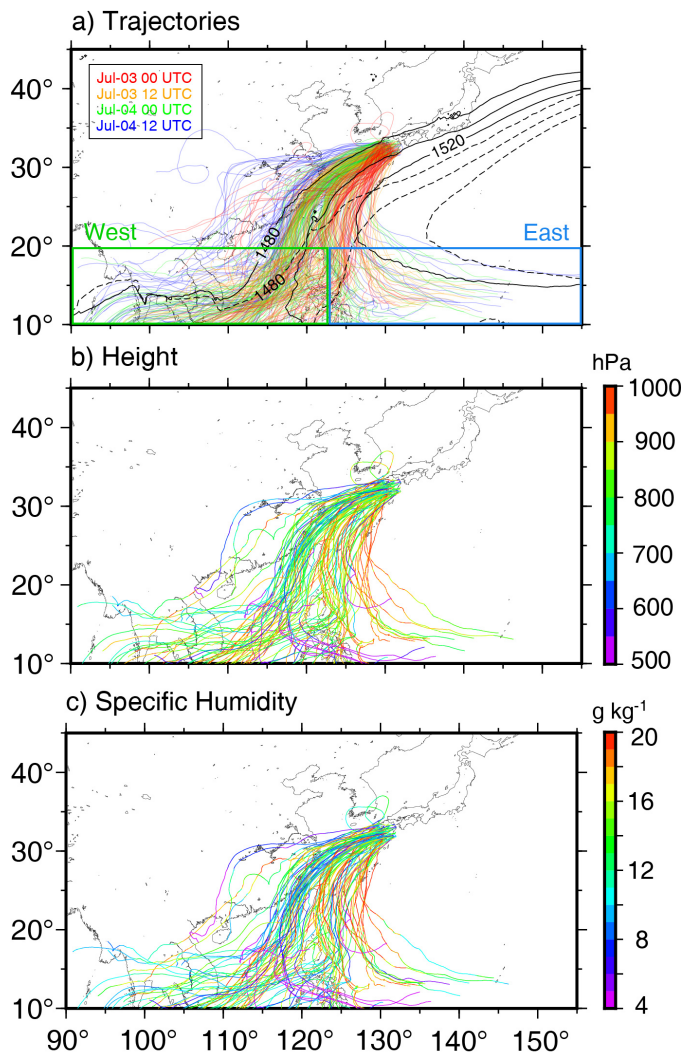
159 where ΔQ_{tot} is the total ‘rain-off’ filtered moisture change, N is the total number of particles
 160 within the atmospheric column over a unit area A (0.5-degree mesh grid in this study). Similarly,
 161 moisture changes ($e - p$) for all particles in the column yielded the net surface freshwater flux
 162 (Romas et al., 2016):

$$163 \quad E - P \approx \frac{\sum_1^N (e-p)}{A}, \quad (4)$$

164 where E is the evaporation rate, P is the precipitation rate.

165 **3 Results**166 **3.1 Moisture transport route**

167 Figure 2a shows the horizontal trajectories of particles (i.e., air parcels). The air parcels
 168 of the 20HR1 mainly came from two tropical regions (Figure 1). Among the 8,868 particles,
 169 6,380 (71.9%) of them came from the regions west of 122 E (the central longitude line of our
 170 domain), including the tropical Indian Ocean (IO) and the regions south of SCS, and 2,285
 171 (25.8%) of particles came from the east (i.e., the tropical Pacific). The amount of water vapor
 172 carried by each particle from the west was lower than those particles from the east when they
 173 reached Kyushu (i.e., the release time). Moreover, our results also showed that all air parcels
 174 became moister during transport (Table S1).



175

176 **Figure 2.** Trajectories of particles colored by the (a) released at different times, (b) pressure and
 177 (c) specific humidity. The mean 850 hPa (1480–1520 gpm) geopotential height are shown by

178 dashed (28th June–1st July) and solid lines (1st July–4th July). To avoid overcrowding, only one of
179 every 100 trajectories was plotted.

180 The trajectories show that most particles travelled within mid-to-lower levels along the
181 periphery of the WPSH, exhibiting a narrow moisture channel (i.e., the AR). This moisture
182 channel varied from time to time, which is likely caused by the changing WPSH. For instance,
183 particles released on 3rd July mainly passed over the East China Sea (ECS) (red curves in Figure
184 2a), while other trajectories shifted westward due to the westward extension of the WPSH in
185 early July (see difference between the solid and dashed lines in Figure 2a). The particles
186 travelling along the edge of WPSH distributed within the whole mid-to-lower troposphere
187 (Figure 2b), while the particles in the east subducted and became moister simultaneous to the
188 dominant WPSH (Figure 2c).

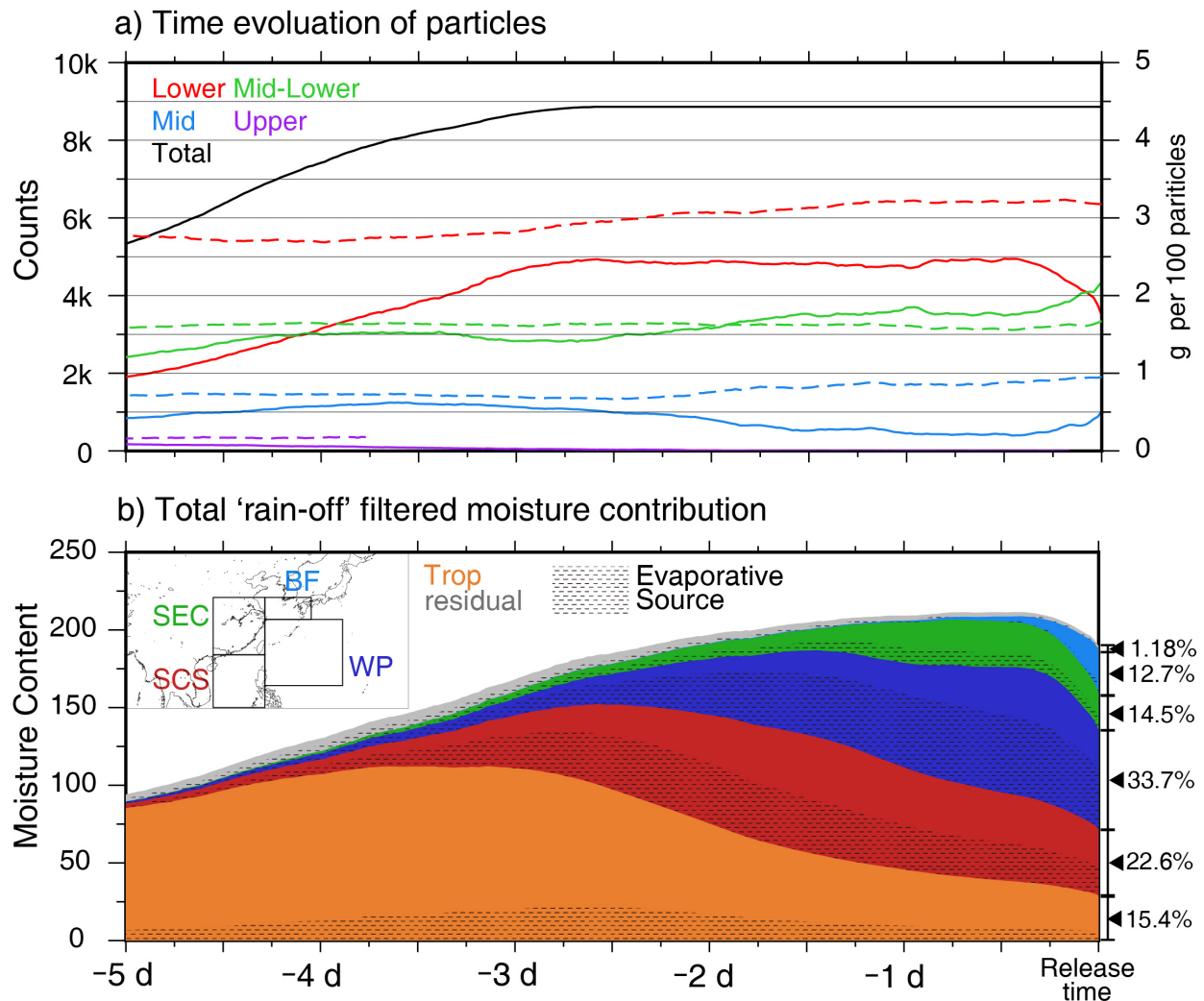
189 The moisture transport route of 20HR1 can be summarized as follows. In the first stage,
190 the air parcels from the tropical IO were transported eastward (and/or northeastward) to the SCS,
191 while other air parcels were transported westward from the tropical Pacific. After merging at
192 approximately 20 N, the air parcels from these two tropical regions went farther north, guided by
193 the WPSH, passing over southeastern China and the WP (and the marginal seas) in next few
194 days. During the northward transport, some air parcels were subducted under the strengthening
195 of WPSH. Within 1 or 2 days, the air parcels encountered the Baiu front at approximately 30 N
196 and turned east along the front before reaching Japan. Readers may refer to an animation that
197 shows the backward tracing of released particles (Video S1; see Data Availability section).

198 3.2 Moisture evolution during transport

199 To further understand the changes in moisture content shown in Figure 2, we examined
200 the vertical distributions and moisture content of particles during transport. For simplicity, we
201 consider the particles in four layers: Lower (> 800 hPa), Mid-Lower (800–600 hPa), Mid (600–
202 400 hPa), and Upper (< 400 hPa). As shown in Figure 3a, the variation trends of the particle
203 numbers of Lower and Mid-Lower layers were quite different, although the numbers of particles
204 were almost the same at both the release time and the end of tracing. More particles were
205 subducted into the Lower layer, which facilitated gains of moisture from the sea surface. As a
206 result, even we ignored the moisture gain-loss cycles, the net water vapor content of particles in
207 the Lower layer increased about 20% during transport (dashed lines in Figure 3a). In contrast,
208 while the particles kept entering the model domain, the particles in the Mid (Mid-Lower) layers
209 decreased (changed only slightly) in numbers with slight change in moisture content, suggesting
210 air parcels more likely subducted into lower levels, which is quite different from the results of
211 ARs formed by WCB-like processes (Bao et al., 2006).

212 Figure 3b shows the time evolution of the ‘rain-off’ filtered moisture contributions of
213 different regions. It is clear that the total moisture content continuously increased until the
214 parcels reached Japan; however, the cause of this increase were different. During the first 2 days
215 (day -5 and day -4), the increase was mainly due to the greater number of particles (hence, the air
216 masses) that entering the domain, especially the low-level air flows(see the black lines in Figure
217 3a). In day -3, after the particles numbers reached its maximum, the amount of moisture from the
218 tropics started decreasing due to the precipitation (the ‘rain-off’), and it declined almost linearly
219 during the next two days. By contrast, more water vapor gained from the SCS and the WP, of
220 which more than half was gained by the evaporation (see masked parts in Figure 3b). Especially,
221 after day -1, the WP played the most important role in the moisture accumulation and finally

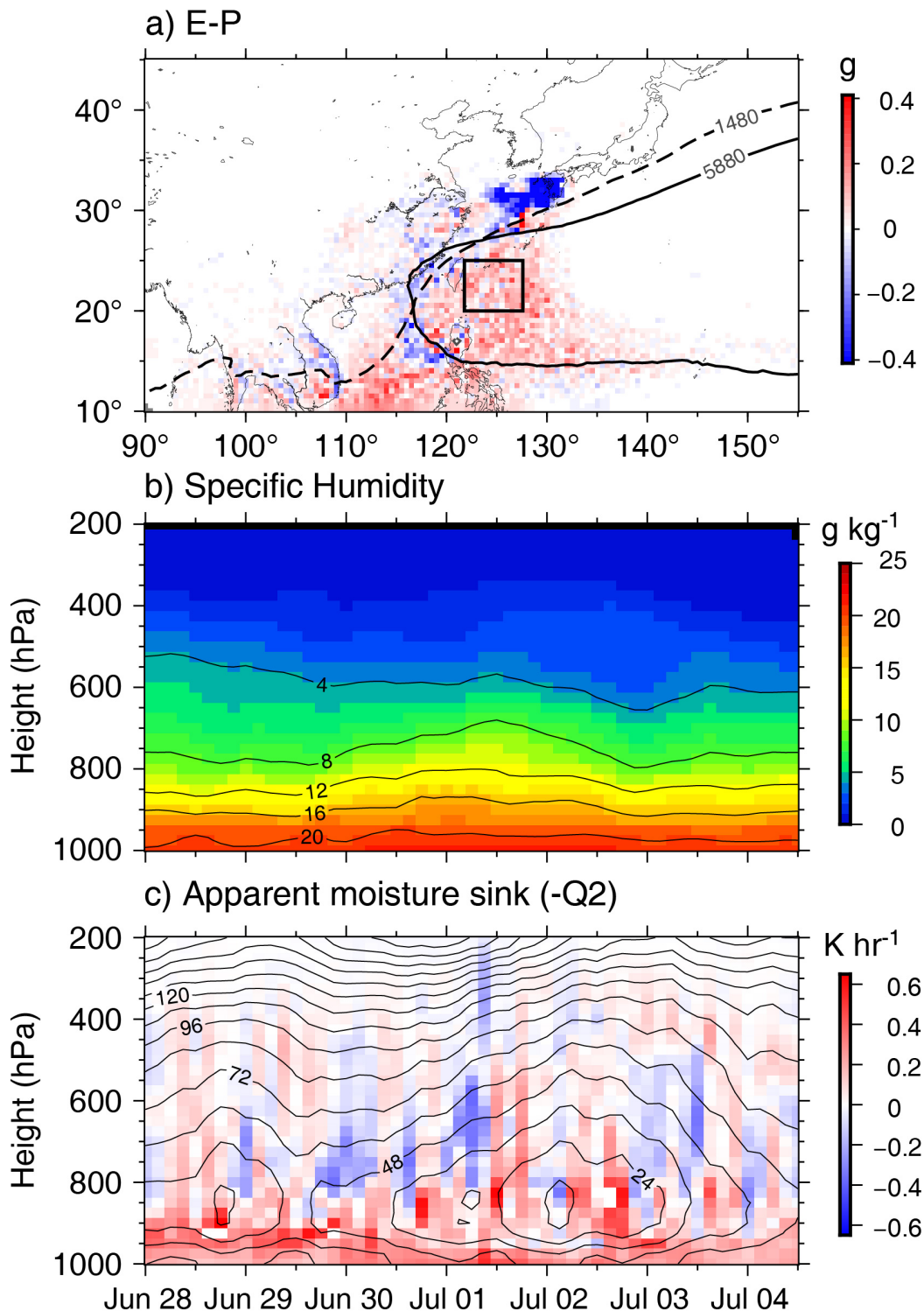
222 contributed 33.7% moisture at day 0 (i.e., release time). Note that the moisture contributed by the
 223 southeast China and the Baiu front was highly related to the heavy rainfalls there, which was
 224 likely caused by the re-evaporation of raindrops and the convective moistening (see the
 225 Subsection 3.3).



226

227 **Figure 3.** Composite time evolutions of (a) particle numbers (solid lines) and moisture (dashed
 228 lines; g per 100 particles) in different layers over the model domain, and (b) the total 'rain-off'
 229 filtered moisture contribution with their final fractions. Note that the 'Trop' includes the 'origin'
 230 moisture and moisture gained in tropical regions (south of 15 N, excluding the SCS).

231 To further show the horizontal distributions of moisture gain/loss processes along the
 232 transport, we evaluated the net surface freshwater fluxes (E-P). The strongest downward
 233 freshwater fluxes (hence, moisture loss) were found around 30 N, indicating heavy rainfall along
 234 the Baiu front (Figure 4a). Moreover, negative values were also found along the periphery of the
 235 WPSH and the coastal region where most of the Mid and Mid-Lower particles travelled (Figure
 236 2b), suggesting that the moisture loss continued due to precipitation along the transport routes. On
 237 the other hand, widely distributed positive freshwater fluxes over the SCS and the WP suggested
 238 the large amount of moisture was gained over those regions, which are consistent with the results
 239 of 'rain-off' filtered contributions (Figure 3b).



240

241 **Figure 4.** (a) The total net freshwater fluxes (E-P, upward positive), while contours show the
 242 WPSH by the mean geopotential height at 850 hPa (dashed) and 500 hPa (solid). (b) Time and
 243 height diagram of the area-averaged specific humidity and (c) apparent moisture sink ($-Q_2$,
 244 positive means increase of moisture) with meridional geopotential height anomalies (contours)
 245 over the region (122.5–127.5 E, 20–25 N; black box in panel a).

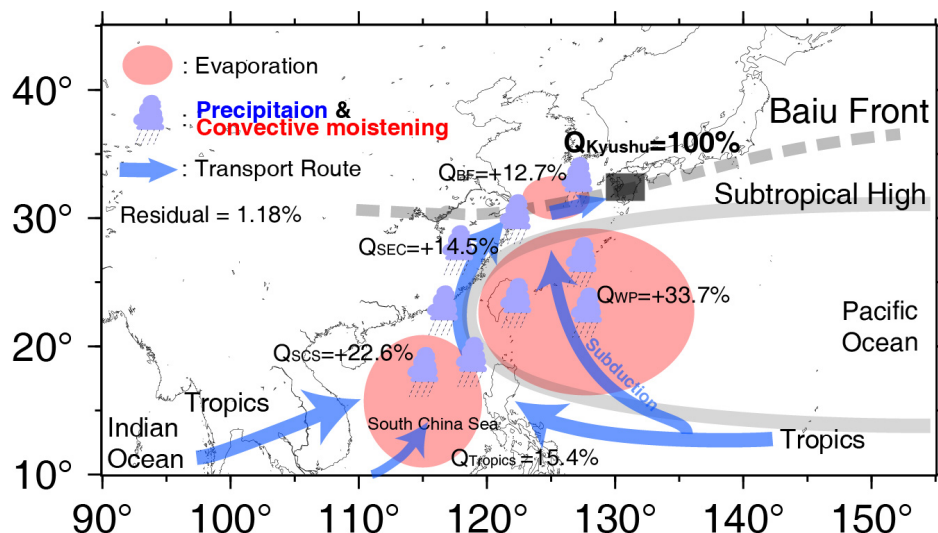
246 3.3 Moistening processes

247 As shown in Figure 3b, about half of moisture was gained from non-evaporative sources
 248 over the subtropics. To reveal what processes helped such moistening, we examined the temporal
 249 variations in humidity and apparent moisture sink (Q_2 ; e.g., Yanai et al., 1973; von Salzen et al.,
 250 2005) over the WP (see black box in Figure 4a). Figure 4b shows that rapid moistening occurred
 251 at lower levels from June 30th to July 3rd, when the top of the high humidity layer ($> 8 \text{ g kg}^{-1}$)
 252 rose from 800 hPa to 700 hPa. The upward moisture transport showed good agreement with
 253 convection (see $-Q_2$ in Figure 4c; positive means moistening), exhibiting the environmental
 254 moistening by convection similar to that reported in tropical studies (e.g., Takemi, 2015).
 255 Although convection mostly remained shallow over this region due to the dominant WPSH (no
 256 clear precipitation, figure not shown), it facilitated lower troposphere moistening and boundary
 257 layer thickening.

258 It is now clear that the non-evaporative moistening over the WP was caused by the low-
 259 to-mid level convection along the moisture channel, and the moistened air parcels were then
 260 transported to Kyushu by low level flows and contributed to the moisture accumulation. Our
 261 analyses also shows that such high humidity low level flows may further enhance the quasi-
 262 stationary line shaped precipitation systems via the “back building” process and, therefore, the
 263 heavy rain in Kyushu (e.g., Schumacher & Johnson, 2005; Manda et al., 2014; See Text S3 for
 264 the analyses).

265 **5 Conclusions**

266 This study investigated the moisture sources and transport processes of the high
 267 accumulation of moisture associated with the heavy rains in July 2020, based on numerical
 268 hindcast and backward trajectory analyses. The 10000 particles with random masses were
 269 released from 3 July, 00:00 UTC to 4 July, 12:00 UTC, and 8,868 particles that originated south
 270 of 30 N were used for the analyses.



271
 272 **Figure 5.** Schematic diagram for the transport route and contribution of the accumulated
 273 moisture during the 20HR1.

274 The backward trajectories exhibit a narrow moisture channel that started from the SCS at
 275 20 N where most particles merged there. This channel was found to be located along the

276 periphery of the WPSH before encountering the Baiu front. Our finding about the moisture
277 sources and transport are summarized schematically in Figure 5. There were two kinds of
278 sources: (a) the moisture transported from tropical regions, including the IO, south of SCS and
279 tropical Pacific, and (b) the moisture gained in subtropics during the transport. The moisture
280 from tropical regions was continuously lost due to precipitation, resulting in a smaller
281 contribution to the final moisture accumulation of 20HR1. Besides the evaporation, our analyses
282 suggest that the air parcels acquired half of moisture via the lower tropospheric convection,
283 especially over the WP where they subducted. Finally, the moisture from tropics (15%) and
284 subtropics (85%) were accumulated as the form of AR along the Baiu front and contributed to
285 the heavy rainfall in Kyushu.

286 The current study demonstrates that, rather than the moisture from the tropics, subtropical
287 regions played the most important role in moisture accumulation and the heavy rain. Moreover,
288 unlike the ARs that formed by the WCB-like ascending background airflows in the winter
289 extratropical cyclones (e.g., Bao et al 2006; Sodemann & Stohl, 2013), the non-evaporative
290 atmosphere moistening in subtropical regions was mainly induced by the self-constructed
291 convection, even under the WPSH.

292 Although we revealed how was the moisture accumulated and transported to Japan, this
293 study was mainly based on one major event during the heavy rains of July 2020; multi-casts and
294 longer simulations could reduce the potential uncertainties. On the other hand, our study also
295 suggests potential impacts of recent increasing sea surface temperatures over the subtropical WP
296 (e.g., Bulgin et al. 2020) on the recorded heavy rainfall in Japan by enhancing the local
297 evaporation and convection. These will be investigated as the next step of this study.

298 **Acknowledgments**

299 The authors are grateful to the quick analysis by Youichi Kamae (University of Tsukuba) and
300 quick report by JMA on the 20HR. This work was partially supported by JSPS KAKENHI
301 (JP19H05697 and JP17H02958) and the Collaborative Research Program (2020 S2-6) of RIAM,
302 Kyushu University.

303 **Data Availability**

304 The data used in this study were listed with the website URL as follows: GSMaP
305 (<https://sharaku.eorc.jaxa.jp/GSMaP>), GDAS/FNL (<https://rda.ucar.edu/datasets/ds083.3>), the
306 ERA5 (<https://cds.climate.copernicus.eu/>), GMPE (<http://marine.copernicus.eu>), and TRMM
307 (<https://gpm.nasa.gov/data/directory>). The trajectories used in this study and the trajectories
308 animation are available on Zenodo.org (<https://doi.org/10.5281/zenodo.3986631> and
309 <https://doi.org/10.5281/zenodo.4027542>, respectively).

310 **References**

311 Bao, J.-W., Michelson, S. A., Neiman, P. J., Ralph, F. M., & Wilczak, J. M. (2006).
312 Interpretation of enhanced integrated water vapor bands associated with extratropical
313 cyclones: Their formation and connection to tropical moisture. *Monthly Weather Review*,
314 134, 1063–1080, <https://doi.org/10.1175/MWR3123.1>

- 315 Brioude, J., Arnold, D., Stohl, A., Cassiani, M., Morton, D., Seibert, P., et al. (2013). The
316 Lagrangian particle dispersion model FLEXPART-WRF version 3.1, *Geoscientific Model*
317 *Development*, 6, 1889–1904, doi:10.5194/gmd-6-1889-2013
- 318 Bulgin, C.E., Merchant, C.J. & Ferreira, D. (2020). Tendencies, variability and persistence of sea
319 surface temperature anomalies. *Scientific Reports*, 10, 7986, doi:10.1038/s41598-020-
320 64785-9
- 321 Copernicus Climate Change Service (C3S) (2017). ERA5: Fifth generation of ECMWF
322 atmospheric reanalyses of the global climate. Copernicus Climate Change Service
323 Climate Data Store (CDS), <https://cds.climate.copernicus.eu>, last accessed on 21 July
324 2020.
- 325 Emergency Operations Center of Japan (EOCJ) (2020). The damage situation during the heavy
326 rain of July 2020 (in Japanese), Report on 7 August 2020, EOCJ, available online:
327 www.bousai.go.jp/updates/r2_07ooame/pdf/r20703_ooame_33.pdf
- 328 Gimeno, L., Stohl, A., Trigo, R. M., Dominguez, F., Yoshimura, K., Yu, L., et al. (2012).
329 Oceanic and terrestrial sources of continental precipitation, *Reviews of Geophysics*, 50,
330 RG4003, doi:10.1029/2012RG000389
- 331 Grell, G. A., & Freitas, S. R. (2014). A scale and aerosol aware stochastic convective
332 parameterization for weather and air quality modeling, *Atmospheric Chemistry and*
333 *Physics*, 14, 5233–5250, doi:10.5194/acp-14-5233-2014
- 334 Guan, B., & Waliser, D. E. (2019). Tracking Atmospheric Rivers Globally: Spatial Distributions
335 and Temporal Evolution of Life Cycle Characteristics, *Journal of Geophysical Research:*
336 *Atmospheres*, 124, 12,523–12,552. <https://doi.org/10.1029/2019JD031205>
- 337 Hirota, N., Takayabu, Y. N., Kato, M., & Arakane, S. (2016). Roles of an Atmospheric River
338 and a Cutoff Low in the Extreme Precipitation Event in Hiroshima on 19 August 2014,
339 *Monthly Weather Review*, 144, 1145–1160, doi:10.1175/MWR-D-15-0299.1
- 340 Hong, S. Y., & Lim, J. O. J. (2006). The WRF single–moment 6–class microphysics scheme
341 (WSM6), *Journal of the Korean Meteorological Society*, 42, 129–151.
- 342 Hong, S. Y., Noh, Y., & Dudhia, J. (2006). A new vertical diffusion package with an explicit
343 treatment of entrainment processes, *Monthly Weather Review*, 134, 2318–2341,
344 doi:10.1175/MWR3199.1
- 345 Iacono, M. J., Delamere, J. S., Mlawer, E. J., Shephard, M. W., Clough, S. A., & Collins, W. D.
346 (2008). Radiative forcing by long–lived greenhouse gases: Calculations with the AER
347 radiative transfer models, *Journal of Geophysical Research*, 113, D13103,
348 doi:10.1029/2008JD009944
- 349 Japan Meteorological Agency (JMA) (2020). Characteristics of the heavy rain of July 2020 and
350 related atmospheric circulation (in Japanese), Press Release on 31 July 2020, JMA,
351 available online: www.jma.go.jp/jma/press/2007/31a/r02gou.pdf
- 352 Jimenez, P. A., Dudhia, J., Gonzalez–Rouco, J. F., Navarro J., Montavez, J. P., & Garcia–
353 Bustamante, E. (2012). A revised scheme for the WRF surface layer formulation,
354 *Monthly Weather Review*, 140, 898–918. doi:10.1175/MWR-D-11-00056.1

- 355 Kamae, Y. (@YKamae_JP) (2020). The heavy rain of July 2020,
356 twitter.com/i/events/1280712104467550209, *Twitter*, last access: 13 September 2020.
- 357 Langhamer, L., Sauter, T., & Mayr, G. J. (2018). Lagrangian Detection of Moisture Sources for
358 the Southern Patagonia Icefield (1979–2017), *Frontiers in Earth Science*, 6, 219,
359 doi:10.3389/feart.2018.00219
- 360 Lavers, D. A., Villarini, G., Allan, R. P., Wood, E. F., & Wade, A. J. (2012). The detection of
361 atmospheric rivers in atmospheric reanalyses and their links to British winter floods and
362 the large-scale climatic circulation, *Journal of Geophysical Research*, 117, D20106,
363 doi:10.1029/2012JD018027
- 364 Manda, A., Nakamura, H., Asano, N., Iizuka, S., Miyama, T., Moteki, Q., et al. (2014). Impacts
365 of a warming marginal sea on torrential rainfall organized under the Asian summer
366 monsoon, *Scientific Reports*, 4, DOI:10.1038/srep05741
- 367 Martin, M., Dash, P., Ignatov, A., Banzon, V., Beggs, H., Brasnett, B., et al. (2012). Group for
368 High Resolution Sea Surface temperature (GHRSSST) analysis fields inter-comparisons.
369 Part 1: A GHRSSST multi-product ensemble (GMPE), *Deep-Sea Research Part II*, 77-80,
370 21–30, doi:10.1016/j.dsr2.2012.04.013
- 371 Naoi, M., Kamae, Y., Ueda, H., & Mei, W. (2020). Impacts of seasonal transitions of ENSO on
372 atmospheric river activity over East Asia, *Journal of the Meteorological Society of Japan*,
373 98, 655–668, doi:10.2151/jmsj.2020-027
- 374 NCEP/NWS/NOAA/U.S. Department of Commerce (2015). NCEP GDAS/FNL 0.25 Degree
375 Global Tropospheric Analyses and Forecast Grids. Research Data Archive at the National
376 Center for Atmospheric Research, Computational and Information Systems Laboratory,
377 doi:10.5065/D65Q4T4Z. Last accessed on 21 July 2020.
- 378 Ramos, A. M., Nieto, R., Tomé, R., Gimeno, L., Trigo, R. M., Liberato, M. L. R., & Lavers, D.
379 A. (2017). Atmospheric rivers moisture sources from a Lagrangian perspective, *Earth
380 System Dynamics*, 7, 371–384, doi:10.5194/esd-7-371-2016
- 381 Sampe, T., & Xie, S. P. (2012). Large-scale dynamics of the Meiyu-Baiu rainband:
382 Environmental forcing by the Westerly Jet, *Journal of Climate*, 23, 1, 113-134,
383 doi:10.1175/2009JCLI3128.1
- 384 Schumacher, R. S., & Johnson, R. H. (2005). Organization and Environmental Properties of
385 Extreme-Rain-Producing Mesoscale Convective Systems, *Monthly Weather Review*, 133,
386 961–976, doi:10.1175/MWR2899.1
- 387 Shimpo, A., Takemura, K., Wakamatsu, S., Togawa, H., Mochizuki, Y., Takekawa, M., et al.
388 (2019). Primary Factors behind the Heavy Rain Event of July 2018 and the Subsequent
389 Heat Wave in Japan, *Scientific Online Letters on the Atmosphere*, 15A, 13–18,
390 doi:10.2151/sola.15A-003
- 391 Stohl, A., & James, P. (2004). A Lagrangian Analysis of the Atmospheric Branch of the Global
392 Water Cycle. Part I: Method Description, Validation, and Demonstration for the August
393 2002 Flooding in Central Europe, *Journal of Hydrometeorology*, 5 (4), 656–678,
394 doi:10.1175/1525-7541(2004)005<0656:ALAOTA>2.0.CO;2

- 395 Sodemann, H., Schwierz, C., & Wernli, H. (2008). Interannual variability of Greenland winter
396 precipitation sources: Lagrangian moisture diagnostic and North Atlantic Oscillation
397 influence, *Journal of Geophysical Research*, 113, D03107, doi:10.1029/2007JD008503
- 398 Sodemann, H., & A. Stohl, A. (2013). Moisture origin and meridional transport in atmospheric
399 rivers and their association with multiple cyclones. *Monthly Weather Review*, 141, 2850-
400 2868. <https://doi.org/10.1175/MWR-D-12-00256.1>
- 401 Takemi, T. (2015). Relationship between cumulus activity and environmental moisture during
402 the CINDY2011/DYNAMO field experiment as revealed from convection-resolving
403 simulations, *Journal of the Meteorological Society of Japan*, 93A, 41-58,
404 doi:10.2151/jmsj.2015-035
- 405 Tewari., M., Chen, F., Wang, W., Dudhia, J., LeMone, M., Mitchell, K., et al. (2004).
406 Implementation and verification of the unified Noah land surface model in the WRF
407 model, 20th Conference on Weather Analysis and Forecasting/16th Conference on
408 Numerical Weather Prediction. 11-15 January, 2004, Seattle, Washington.
- 409 Tsuguti, H., Seino, N., Kawase, H., Imada, Y., Nakaegawa, T., & Takayabu, I. (2019).
410 Meteorological overview and mesoscale characteristics of the Heavy Rain Event of July
411 2018 in Japan, *Landslides*, 16, 363–371, doi:10.1007/s10346-018-1098-6, 2019
- 412 Tsuji, H., & Takayabu, Y. N. (2019). Precipitation Enhancement via the Interplay between
413 Atmospheric Rivers and Cutoff Lows, *Monthly Weather Review*, 147, 2451–2466,
414 doi:10.1175/MWR-D-18-0358.1
- 415 von Salzen, K., McFarlane, N. A., & Lazare, M. (2015). The role of shallow convection in the
416 water and energy cycles of the atmosphere, *Climate Dynamics*, 25, 671–688,
417 doi:10.1007/s00382-005-0051-2
- 418 NHK World News (2020). Kuma River overflow leads to extensive flooding., *NHK World News*
419 – *At a Glance*, <https://www3.nhk.or.jp/nhkworld/en/news/ataglance/1030/>, last accessed:
420 13 September 2020.
- 421 Yanai, M., Esbensen, S., & Chu, J. H. (1973). Determination of bulk properties of tropical cloud
422 clusters from large scale heat and moisture budgets, *Journal of the Atmospheric Sciences*,
423 30 (4), 611–627. doi: 10.1175/765 1520-0469(1973)030h0611:DOBPOTi2.0.CO;2
- 424 Zhong, R. (2020). Severe Floods in China Leave Over 106 Dead or Missing, *The New York*
425 *Times*, <https://www.nytimes.com/2020/07/03/world/asia/china-floods-rain.html>, last
426 access: 13 September 2020, 2020.
- 427 Zhou, T. J., & Yu, R. C. (2005). Atmospheric water vapor transport associated with typical
428 anomalous summer rainfall patterns in China, *Journal of Geophysical Research*, 110,
429 D08104, doi:10.1029/2004JD005413

430 **References from the Supporting Information**

- 431 Dudhia, J., (1989). Numerical study of convection observed during the Winter Monsoon
432 Experiment using a mesoscale two–dimensional model. *Journal of the Atmospheric*
433 *Sciences*, 46, 3077–3107. doi:10.1175/1520-0469(1989)046<3077:NSOCOD>2.0.CO;2

- 434 Huffman, G., Bolvin, D., Braithwaite, D., Hsu, K., Joyce, R., Xie, P. (2014). Integrated Multi-
435 satellitE Retrievals for GPM (IMERG), version 4.4. NASA's Precipitation Processing
436 Center, accessed 1st August, 2020, <ftp://arthurhou.pps.eosdis.nasa.gov/gpmdata/>
- 437 Kubota, T., Aonashi, K., Ushio, T., Shige, S., Takayabu, Y. N., Kachi, M., et al. (2020). Global
438 Satellite Mapping of Precipitation (GSMaP) products in the GPM era. In V. Levizzani, C.
439 Kidd, D. Kirschbaum, C. Kummerow, K. Nakamura, F. Turk (Eds.), *Satellite*
440 *precipitation measurement* (Vol. 67, pp. 355–373), Switzerland, Springer,
441 doi:10.1007/978-3-030-24568-9_20
- 442 Langhamer, L., Sauter, T., & Mayr, G. J. (2018). Lagrangian Detection of Moisture Sources for
443 the Southern Patagonia Icefield (1979–2017), *Frontiers in Earth Science*, 6, 219,
444 doi:10.3389/feart.2018.00219
- 445 Mlawer, E. J., Taubman, S. J., Brown, P. D., Iacono, M. J., & Clough, S. A. (1997). Radiative
446 transfer for inhomogeneous atmospheres: RRTM, a validated correlated-k model for the
447 longwave. *Journal of Geophysical Research*, 102, 16663–16682. doi:10.1029/97JD00237
- 448 Olson, J. B., Kenyon, J. S., Angevine, W. M., Brown, J. M., Pagowski, M., & Sušelj, K. (2019).
449 A Description of the MYNN-EDMF Scheme and the Coupling to Other Components in
450 WRF–ARW. *NOAA Technical Memorandum OAR GSD*, 61, 37, doi:10.25923/n9wm-
451 be49
- 452 Schumacher, R. S., & Johnson, R. H. (2005). Organization and Environmental Properties of
453 Extreme-Rain-Producing Mesoscale Convective Systems. *Monthly Weather Review*, 133,
454 961–976, <https://doi.org/10.1175/MWR2899.1>.
- 455 Shinoda, T., Uyeda, H., & Yoshimura, K. (2005). Structure of Moist Layer and Sources of Water
456 over the Southern Region Far from the Meiyu/Baiu Front, *Journal of the Meteorological*
457 *Society of Japan*, 83, 2, 137-152, doi:10.2151/jmsj.83.137
- 458 Sodemann, H., Schwierz, C., & Wernli, H. (2008). Interannual variability of Greenland winter
459 precipitation sources: Lagrangian moisture diagnostic and North Atlantic Oscillation
460 influence, *Journal of Geophysical Research*, 113, D03107, doi:10.1029/2007JD008503
- 461 Tao, W.-K., Wu, D., Lang, S., Chern, J.-D., Peters-Lidard, C., Fridlind, A., & Matsui, T. (2016).
462 High-resolution NU-WRF simulations of a deep convective-precipitation system during
463 MC3E: Further improvements and comparisons between Goddard microphysics schemes
464 and obser- vations. *Journal of Geophysical Research: Atmospheres*, 121, 1278–1305.
465 doi:10.1002/2015JD023986.
- 466 Tu, C. C., Chen, Y. L., Lin, P. L., & Lin, P. H. (2020). The relationship between the boundary
467 layer moisture transport from the South China Sea and heavy rainfall over Taiwan,
468 *Terrestrial Atmospheric and Oceanic Sciences*, 31, 159-176, doi:
469 10.3319/TAO.2019.07.01.01